Available online at www.sciencedirect.com
ScienceDirect
Journal of Solid State Chemistry 180 (2007) 2558–2565
JOURNAL OF SOLID STATE CHEMISTRY
www.elsevier.com/locate/jssc

The disordered structures and low temperature dielectric relaxation properties of two misplaced-displacive cubic pyrochlores found in the Bi_2O_3–$M^{II}O$–Nb_2O_5 (M = Mg, Ni) systems

Hai Binh Nguyen[a], Lasse Norén[a], Yun Liu[a], Ray L. Withers[a,*], Xiaoyong Wei[b], Margaret M. Elcombe[c]

[a]*Research School of Chemistry, Australian National University, Canberra, ACT 0200, Australia*
[b]*Electronic Materials Research Laboartory (EMRL), Xian Jiaotong University, Xian, Shaanxi 710049, China*
[c]*The Bragg Institute, Building 87, Australian Nuclear Science and Technology Organisation PMB, Menai, NSW 2234, Australia*

Received 7 May 2007; received in revised form 3 July 2007; accepted 4 July 2007
Available online 13 July 2007

Abstract

The disordered structures and low temperature dielectric relaxation properties of $Bi_{1.667}Mg_{0.70}Nb_{1.52}O_7$ (BMN) and $Bi_{1.67}Ni_{0.75}Nb_{1.50}O_7$ (BNN) misplaced-displacive cubic pyrochlores found in the Bi_2O_3–$M^{II}O$–Nb_2O_5 (M = Mg, Ni) systems are reported. As for other recently reported Bi-pyrochlores, the metal ion vacancies are found to be confined to the pyrochlore A site. The B_2O_6 octahedral sub-structure is found to be fully occupied and well-ordered. Considerable displacive disorder, however, is found associated with the $O'A_2$ tetrahedral sub-structure in both cases. The A-site ions were displaced from Wyckoff position 16d ($\frac{1}{2}$, $\frac{1}{2}$, $\frac{1}{2}$) to 96 h ($\frac{1}{2}$, $\frac{1}{2}-\varepsilon_A$, $\frac{1}{2}+\varepsilon_A$) while the O′ oxygen was shifted from position 8b ($\frac{3}{8}$, $\frac{3}{8}$, $\frac{3}{8}$) to Wyckoff position 32e ($\frac{3}{8}+\varepsilon'_O$, $\frac{3}{8}+\varepsilon'_O$, $\frac{3}{8}+\varepsilon'_O$). The refined displacement magnitudes off the 16d and 8b sites for the A and O′ sites were 0.408 Å/0.423 Å and 0.350 Å/0.369 Å for BMN/BNN, respectively.

Keywords: Powder neutron diffraction; Disordered structure refinement; Bi-pyrochlores; Dielectric relaxation

1. Introduction

Bi-based, cubic pyrochlore phases have been of considerable interest over recent years as a result of their relatively high (as well as electric field tuneable) dielectric constants and low dielectric losses over a considerable frequency range around room temperature coupled with their relatively low sintering temperatures, enabling the possibility of co-firing with, e.g. Ag electrodes [1–6]. This combination of properties makes such materials attractive candidates for multilayer capacitor and integrated device applications [5,6]. By far the most attention to date has focussed on a $Bi_{1.5}Zn_{1-\delta}Nb_{1.5}O_{7-\delta}$ (BZN) cubic pyrochlore phase found in the Bi_2O_3–$Zn^{II}O$–Nb_2O_5 ternary oxide system [5–10] as a result of the fact that its temperature coefficient of capacitance can be tuned close to zero (a further requirement for practical applications) when used in conjunction with a nearby monoclinic zirconolite-like $Bi_2(Zn_{2/3}Nb_{4/3})O_7$ ternary phase [3].

Crystal chemical interest in these Bi-based pyrochlores has simultaneously arisen as a result of careful phase analysis studies in BZN and several other such systems [9–13] showing that they do not form at 'sensible' stoichiometries such as $Bi_2(M^{II}_{2/3}Nb^{V}_{4/3})O_7$ or $Bi_2(M^{III}Nb^{V})O_7$ but rather appear to be significantly Bi-deficient with respect to these ideal stoichiometries and to require the presence of nominally far too small M^{2+} or M^{3+} cations on the A sites (as well as the B sites) of the ideal $A_2B_2O_7$ (or $B_2O_6 \cdot O'A_2$) pyrochlore structure type (shown in Fig. 1). This has led to their designation as so-called "misplaced-displacive" cubic pyrochlores [10]. Structure refinements of BZN [7–9] and a few other such Bi-based pyrochlores [11–13] to date have all reported considerable displacive disorder, particularly associated with the $O'A_2$ sub-structure. Despite considerable recent efforts, however, the local crystal chemistry underlying

*Corresponding author. Fax: +61 2 6125 0750.
E-mail address: withers@rsc.anu.edu.au (R.L. Withers).

0022-4596/$ - see front matter © 2007 Elsevier Inc. All rights reserved.
doi:10.1016/j.jssc.2007.07.003

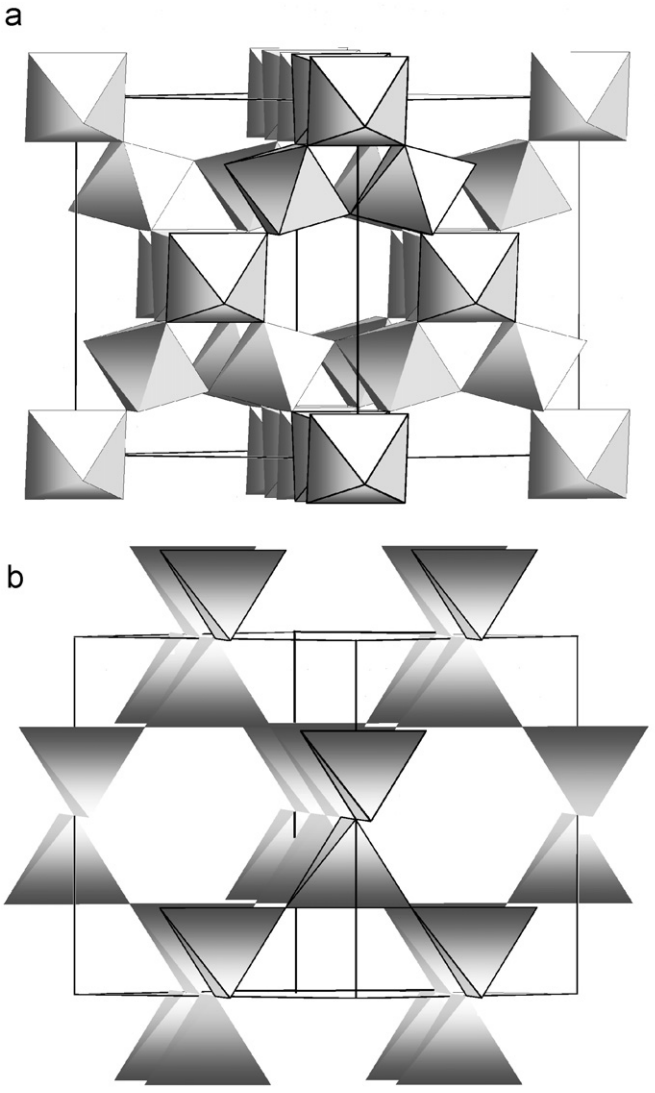

Fig. 1. The ideal pyrochlore $A_2B_2O_7$ or $B_2O_6.O'A_2$ structure type projected along a close to ⟨110⟩ direction. The B_2O_6 octahedral framework sub-structure is shown in (a) and the $O'A_2$ tetrahedral framework sub-structure in (b).

such behaviour still remains far from well understood [7,8,14,15]. The apparently inherent (compositional and coupled) displacive disorder of these Bi-pyrochlore phases is important to understand both from the fundamental crystal chemical point of view but also because it has been linked to anomalous low temperature, glass-like dielectric relaxation behaviour in these systems which has the potential to rule out their use in the RF/microwave frequency range [2,5,16,17].

In this paper, we report the disordered structures of two further Bi-based cubic pyrochlore phases found in the Bi_2O_3–$M^{II}O$–Nb_2O_5 (M = Mg and Ni) systems, labelled BMN and BNN, respectively, in what follows, as well as their low temperature dielectric relaxation behaviour. In the case of the M^{II} = Ni system, Valant and Suvorov [18] very recently carried out a detailed phase analysis investigation and report the existence of a quite compact cubic pyrochlore solid solution field with a composition centred around $Bi_{1.5}Ni_{0.667}Nb_{1.333}O_{6.25}$ (or $Bi_{1.68}Ni_{0.747}Nb_{1.493}O_7$ if normalized to seven oxygens) rather than the $Bi_2(Ni_{2/3}Nb_{4/3})O_7$ composition assumed by Cann et al. [2] or the $Bi_{1.5}Ni_{1.0}Nb_{1.5}O_7$ composition reported by Sirotinkin and Bush [19]. Our own recent synthesis and electron diffraction study of this BNN phase [20] is in agreement with the metal ion ratios reported by Valant and Suvorov [18]. It is not, however, possible to tell without a full structure refinement whether the $Bi_{1.5}Ni_{0.667}Nb_{1.333}O_{6.25}$ or the re-normalized $Bi_{1.68}Ni_{0.747}Nb_{1.493}O_7$ composition is correct and, hence, whether the A site necessarily contains Ni^{2+} ions or not.

In the case of the M^{II} = Mg system, there has yet to be a detailed phase analysis investigation of the location and extent of the cubic pyrochlore solid solution field. Our own recent synthesis and electron diffraction investigation [20] found a cubic pyrochlore BMN phase with an electron microprobe determined composition of $Bi_{1.67}Mg_{0.64}Nb_{1.53}O_7$ (the apparent Mg-deficiency relative to the nominal composition reported in [20] was later found to be due to insufficient drying of the MgO starting powder prior to weighing). The sample, however, also contained a trace amount of a second phase. Synthesis at a slightly more Mg-rich composition (see below) was subsequently found to give a pure single phase cubic pyrochlore sample. As in the case of the M^{II} = Ni system, a full structure refinement of this BMN sample is needed in order to confirm its stoichiometry and whether the A site necessarily contains Mg^{2+} ions or not.

2. Experimental

2.1. Synthesis and initial characterization

Samples of nominal stoichiometry $Bi_{1.667}Mg_{0.70}Nb_{1.52}O_7$ (BMN) and $Bi_{1.667}Ni_{0.75}Nb_{1.5}O_7$ (BNN) were synthesized from high purity Bi_2O_3, MgO or NiO and Nb_2O_5 oxide starting materials, following standard solid-state reaction procedures. Powdered oxides at the nominal stoichiometry were first dried, then mixed and homogenised through grinding in an agate mortar under acetone for 30 min. This resultant mixture was then dried, pressed to pellets and calcined in air at 800 °C overnight using a Pt-crucible as the reaction vessel. The pellets were then re-ground, re-pelleted and sintered at 1050 °C for a further 3 days for both samples.

The purity of the resultant materials was checked via powder XRD using Cu$K\alpha_1$ radiation and the Guinier–Hägg camera technique. High purity Si powder (Lot GD#1 [21], a = 5.43011(5) Å) was added as an internal standard for accurate determination of the unit cell parameters, refined using the program "Unitcell" [22]. The samples were both found to be single phase cubic pyrochlores with a = 10.5653(4) Å for the BMN sample and 10.5440(4) Å for the BNN sample.

The composition of the samples were also checked via electron probe microanalysis (EPMA), using a JEOL 6400 scanning electron microscope (SEM) equipped with an Oxford Instruments light element EDS detector and Link ISIS SEMquant software. Multiple spot analyses were carried out at 15 kV and 1 nA using $BiNbO_4$, MgO and NiO as standards. The obtained average compositions (20 separate spot analyses) were: $Bi_{1.66(1)}Ni_{0.73(3)}Nb_{1.51(2)}O_7$ (O not refined) for the BNN sample and $Bi_{1.66(1)}Mg_{0.70(3)}Nb_{1.52(1)}O_7$ (O not refined) for the BMN sample. Both are in good agreement with the starting compositions. As the BMN and BNN samples were also both single phase to XRD, the compositions of the samples were taken to be the above nominal starting compositions in the following refinements.

2.2. Neutron diffraction/refinement

Room temperature (298 K) powder neutron diffraction data of both samples were collected on the high-resolution powder diffractometer (HRPD) at the high flux Australian reactor (HIFAR) at a wavelength of ~1.49 Å [23]. The samples were placed in a vanadium canister of 10 mm diameter and continuously rotated during data collection carried out in 0.05° steps between 0.027° and 150.027° in 2θ. The Rietica for Windows software package [24] was used for Rietveld structural refinement. Data below 8° and above 150° in 2θ were treated as excluded regions. The unit cell values obtained for BMN and BNN via XRD were used as "standards" to refine the neutron beam wavelength to $\lambda_{neutron} = 1.4913(2)$ Å (given as ~1.49 Å) which was then fixed.

The structural parameters refined were atomic coordinates, site occupancies and atomic displacement parameters (ADPs), both isotropic and anisotropic. The fractional co-ordinates and ADPs for both ions located on the ideal pyrochlore *A* sites (Bi^{3+} and Ni^{2+} or Mg^{2+}) as well as for those on the *B* sites (Ni^{2+} or Mg^{2+} and Nb^{5+}) were always constrained to be equal. The results are detailed in Tables 1 and 2.

2.3. Dielectric properties measurements

Pressed pellets of BMN and BNN samples (diameter 10 mm and thickness 0.3 mm) were polished on both sides.

Table 1
Structural parameters for BMN refined using the four models as described in the text

Atom	Site	x	y	z	U_{iso}*	Occ. (%)
Bi/Mg2	16*d*	$\frac{1}{2}$	$\frac{1}{2}$	$\frac{1}{2}$	0.1004(15)	83.3/11
	16*d*	$\frac{1}{2}$	$\frac{1}{2}$	$\frac{1}{2}$	*a	83.3/11
	96*h*	$\frac{1}{2}$	0.4722(2)	0.5278(2)	0.0180(11)	83.3/11
	96*h*	**$\frac{1}{2}$**	**0.4727(9)**	**0.5273(9)**	***b**	**83.3/11**
Nb/Mg1	16*c*	0	0	0	0.0118(4)	76/24
	16*c*	0	0	0	*c	76/24
	16*c*	0	0	0	0.0116(4)	76/24
	16*c*	**0**	**0**	**0**	***d**	**76/24**
O	48*f*	0.3194(2)	$\frac{1}{8}$	$\frac{1}{8}$	0.0223(4)	100
	48*f*	0.3201(1)	$\frac{1}{8}$	$\frac{1}{8}$	*e	100
	48*f*	0.3193(1)	$\frac{1}{8}$	$\frac{1}{8}$	0.0192(3)	100
	48*f*	**0.3198(1)**	**$\frac{1}{8}$**	**$\frac{1}{8}$**	***f**	**100**
O′	8*b*	$\frac{3}{8}$	$\frac{3}{8}$	$\frac{3}{8}$	0.095(3)	100
	8*b*	$\frac{3}{8}$	$\frac{3}{8}$	$\frac{3}{8}$	*g	100
	32*e*	0.3548(6)	0.3548(6)	0.3548(6)	0.041(4)	100
	32*e*	**0.3559(11)**	**0.3559(11)**	**0.3559(11)**	***h**	**100**

Atom	U_{11}	U_{22}	U_{33}	U_{12}	U_{13}	U_{23}
*a	0.1031(14)	0.1031(14)	0.1031(14)	−0.0452(14)	−0.0452(14)	−0.0452(14)
***b**	**0.025(9)**	**0.025(9)**	**0.018(6)**	**−0.012(11)**	**0.0039(23)**	**0.0039(23)**
*c	0.0168(4)	0.0168(4)	0.0168(4)	−0.00037(5)	−0.00037(5)	−0.00037(5)
***d**	**0.0124(4)**	**0.0124(4)**	**0.0124(4)**	**−0.0031(5)**	**−0.0031(5)**	**−0.0031(5)**
*e	0.0316(8)	0.0165(4)	0.0165(4)	0	0	0.0119(6)
***f**	**0.0281(8)**	**0.0166(4)**	**0.0166(4)**	**0**	**0**	**0.0090(6)**
*g	0.1143(30)	0.1143(30)	0.1143(30)	0	0	0
***h**	**0.062(7)**	**0.062(7)**	**0.062(7)**	**−0.004(3)**	**−0.004(3)**	**−0.004(3)**

The first line for each atom is Model 1, the second line is for Model 2, the third line is for Model 3 and the fourth line is the final Model 4 (in bold). The cubic unit cell was $a = 10.5662(2)$ Å and the space group *Fd*-3*m* (origin choice 2). The anisotropic ADPs are given below the atom coordinates, the refinement statistics are in the text.

Table 2
Structural parameters for BNN re.fined using the four models as described in the text

Atom	Site	x	y	z	U_{iso}*	Occ. (%)
Bi/Ni2	16*d*	$\frac{1}{2}$	$\frac{1}{2}$	$\frac{1}{2}$	0.1086(15)	83.3/12.5
	16*d*	$\frac{1}{2}$	$\frac{1}{2}$	$\frac{1}{2}$	*c	83.3/12.5
	96*h*	$\frac{1}{2}$	0.4713(2)	0.5287(2)	0.0232(11)	83.3/12.5
	96*h*	**$\frac{1}{2}$**	**0.4716(9)**	**0.5284(9)**	***d**	83.3/12.5
Nb/Ni1	16*c*	0	0	0	0.0114(4)	75/25
	16*c*	0	0	0	*a	75/25
	16*c*	0	0	0	0.0096(3)	75/25
	16*c*	**0**	**0**	**0**	***b**	75/25
O	48*f*	0.3194(2)	$\frac{1}{8}$	$\frac{1}{8}$	0.0212(4)	100
	48*f*	0.3202(1)	$\frac{1}{8}$	$\frac{1}{8}$	*g	100
	48*f*	0.3194(1)	$\frac{1}{8}$	$\frac{1}{8}$	0.0178(3)	100
	48*f*	**0.3199(1)**	**$\frac{1}{8}$**	**$\frac{1}{8}$**	***h**	**100**
O'	8*b*	$\frac{3}{8}$	$\frac{3}{8}$	$\frac{3}{8}$	0.1030(31)	100
	8*b*	$\frac{3}{8}$	$\frac{3}{8}$	$\frac{3}{8}$	*e	100
	32*e*	0.3535(5)	0.3535(5)	0.3535(5)	0.0421(36)	100
	32*e*	**0.3548(11)**	**0.3548(11)**	**0.3548(11)**	***f**	**0.975/0.99(2)**

Atom	U_{11}	U_{22}	U_{33}	U_{12}	U_{13}	U_{23}
*a	0.0143(3)	0.0143(3)	0.0143(3)	−0.0021(4)	−0.0021(4)	−0.0021(4)
***b**	**0.0109(3)**	**0.0109(3)**	**0.0109(3)**	**−0.0021(4)**	**−0.0021(4)**	**−0.0021(4)**
*c	0.1137(15)	0.1137(15)	0.1137(15)	−0.0499(11)	−0.0499(11)	−0.0499(11)
***d**	**0.024(8)**	**0.024(8)**	**0.024(8)**	**−0.015(11)**	**0.001(2)**	**0.001(2)**
*e	0.1225(32)	0.1225(32)	0.1225(32)	0	0	0
***f**	**0.067(7)**	**0.067(7)**	**0.067(7)**	**−0.004(3)**	**−0.004(3)**	**−0.004(3)**
*g	0.0299(8)	0.0147(4)	0.0147(4)	0	0	0.0111(5)
***h**	**0.0263(8)**	**0.0151(4)**	**0.0151(4)**	**0**	**0**	**0.0084(6)**

The first line for each atom is Model 1, the second line is for Model 2, the third line is for Model 3 and the fourth line is the final Model 4 (in bold). The refined cubic unit cell parameter $a = 10.5427(2)$ Å and the space group *Fd*-3*m* (origin choice 2). Anisotropic ADPs are given below the atom coordinates and the corresponding refinement statistics in the text.

Their relative density was typically >95%. They were then coated with silver paste for dielectric measurement using a high precision LCR meter (HP4284A) and an environmental box over a temperature range from 325 K down to liquid nitrogen temperature ~90 K. To prevent electrical breakdown along the edge of the pellets, only one side of the pellets were fully coated with silver paste. The remaining side of the pellets was also coated with silver paste, but only partially (to a diameter of 6 mm).

3. Results

3.1. Refinement results

The $A_2B_2O_7$, or $B_2O_6 \cdot O'A_2$, ideal pyrochlore structure type (see Fig. 1) has the *A* cations on 16*d* at $\frac{1}{2},\frac{1}{2},\frac{1}{2}$, the *B* cations on 16*c* at 0 0 0, the O oxygens on 48*f* at $x,\frac{1}{8},\frac{1}{8}$ and the O′ oxygens on 8*b* at $\frac{3}{8},\frac{3}{8},\frac{3}{8}$ (origin setting 2, *Fd*-3*m*). An initial test refinement of the BNN sample assuming a re-normalized $Bi_{1.667}Ni_{0.75}Nb_{1.5}O_7$ stoichiometry similar to that reported in [18] of $Bi_{1.48}(Ni_{2/3}Nb_{4/3})O_{6.22}$ or $O'_{0.22}Bi_{1.48} \cdot (Ni_{2/3}Nb_{4/3}O6)$ (with Ni only on the pyrochlore *B* sites and the O′ site occupied at a very low level) quickly blew up with strongly negative ADPs on the O′ site, etc. It was clear that Ni must occupy both the pyrochlore *A* and *B* sites while the occupancy of the O′ site must be close to one. The same was true for BMN. Subsequent refinements thus assumed $(Bi_{0.833}Mg_{0.11}\square_{0.06})_2(Mg_{0.24}Nb_{0.76})_2O_7$ and $(Bi_{0.833}Ni_{0.125}\square_{0.04})_2(Ni_{0.25}Nb_{0.75})_2O_7$ (□ a vacancy) starting compositions, i.e. no oxygen vacancies and full occupancy of the octahedral metal ion *B* sites.

The initial refinements (model 1, see the first lines of Table 1 for BMN and Table 2 for BNN; BMN: $R_p = 0.0728$; $R_{wp} = 0.0925$; $\chi^2 = 2.878$, D–W: 0.578, 0.785; BNN: $R_p = 0.0708$, $R_{wp} = 0.0910$, $\chi^2 = 2.868$, D–W: 0.527, 0.768) assumed the ideal pyrochlore structure type and isotropic ADPs. The one unknown fractional co-ordinate, the x fractional co-ordinate of the 48*f* oxygen ions, then refined to the same value of 0.3194(2) for both BMN and BNN, in reasonably good agreement with the predicted value of 0.3163 given in [20]. The relative magnitudes of the refined isotropic U_{iso}'s for this model 1 were quite comparable with those refined using the same model for the other Bi-based pyrochlores whose structures

have been refined to date (cf. e.g. with Table 1 of [7,8] and the Model 1 columns of Table 3 of [11,12]). In particular, the refined U_{iso}'s for the B cations and O oxygen making up the B_2O_6 sub-structure are relatively normal while those for the A cations and O′ oxygen constitututing the O′A_2 sub-structure are ~5–10 times larger and clearly abnormal, requiring substantial displacive disorder associated with the O′A_2 sub-structure.

The introduction of anisotropic ADPs (Model 2, the second lines in Tables 1 and 2), in particular on the Bi/M^{2+}, or A site, lead to a significant improvement in refinement statistics (BMN: $R_p = 0.0598$, $R_{wp} = 0.0728$, $\chi^2 = 1.805$, D–W: 1.027, 1.209; BNN: $R_p = 0.0578$, $R_{wp} = 0.0702$, $\chi^2 = 1.709$, D–W: 0.971, 1.243). The principal components of the mean square displacement ellipsoid of the A-site ions along and perpendicular to the local O′–A–O′ direction refined to values given by $U_{11} + 2U_{12} = 0.0127\,\text{Å}^2/0.0139\,\text{Å}^2$ and $U_{11} - U_{12} = 0.1483\,\text{Å}^2/0.1636\,\text{Å}^2$ for BMN/BNN, respectively, i.e. to a very flat, or pancake-shaped, ellipsoid. Clearly, as has also been found for BZN [7–9] and the other Bi-pyrochlores whose structures have been refined to date [9–13], the disordered A cation displacements are constrained to displace in {111} planes perpendicular to the local O′–A–O′-axis (by ~0.385 Å/~0.405 Å in this case).

The next stage of the refinement was to introduce displacive disorder on both the A and O′ sites in order to significantly reduce the isotropic ADPs of the model 1 refinement and in line with earlier structural studies of other Bi-pyrochlores [8,10,11]. The A-site ions were thus displaced from Wyckoff position 16d ($\frac{1}{2}$, $\frac{1}{2}$, $\frac{1}{2}$) to 96h ($\frac{1}{2}$, $\frac{1}{2} - \varepsilon_A$, $\frac{1}{2} + \varepsilon_A$) while the O′ atom was shifted from position 8b ($\frac{3}{8}$, $\frac{3}{8}$, $\frac{3}{8}$) to Wyckoff position 32e ($\frac{3}{8} + \varepsilon'_o$, $\frac{3}{8} + \varepsilon'_o$, $\frac{3}{8} + \varepsilon'_o$). The refined displacement magnitudes off the 16d and 8b sites for the A and O′ sites were then 0.415 Å/0.428 Å and 0.370 Å/0.393 Å for BMN/BNN, respectively. This model (Model 3, the third lines in Tables 1 and 2) significantly reduced the originally refined isotropic ADPs on both the A and O′ sites (although that on the O′ site still remains rather too high suggesting that the disorder on the O′ site is not particularly well-modelled by the splitting employed) while the refinement statistics also improved (BMN: $R_p = 0.0606$, $R_{wp} = 0.0726$, $\chi^2 = 1.775$, D–W: 1.098, 1.231; BNN: $R_p = 0.0578$, $R_{wp} = 0.0697$, $\chi^2 = 1.683$, D–W: 1.052, 1.262). (It is worth noting that the refinement statistics remain virtually identical if the sign of ε'_o is reversed.)

The final refinements (Model 4, line 4 of Tables 1 and 2, see also Figs. 2a and b) kept the displacive disorder on both the A and O′ sites outlined in Model 3 but allowed anisotropic ADPs for all atoms. This introduced an additional seven parameters but lead to a significant further improvement in refinement statistics (BMN: $R_p = 0.0538$, $R_{wp} = 0.0665$, $\chi^2 = 1.508$, D–W: 1.409, 1.437; BNN: $R_p = 0.0534$, $R_{wp} = 0.0648$, $\chi^2 = 1.458$, D–W: 1.301, 1.447) compared to Model 3. Note that the refined anisotropic displacement ellipsoid for the already displaced

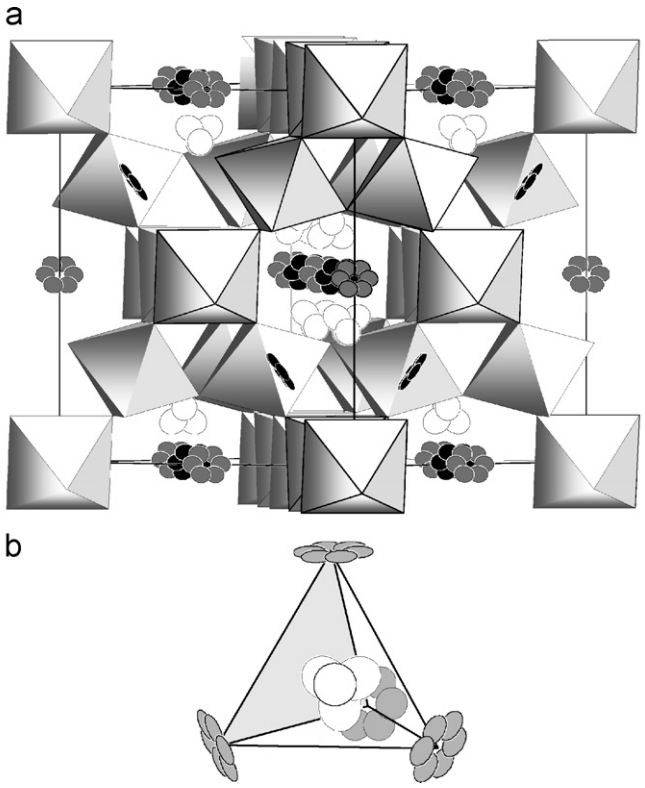

Fig. 2. (a) The final displacively disordered average structure (Model 4, Table 1) for $Bi_{1.667}Mg_{0.70}Nb_{1.52}O_7$ (BMN) projected along a close to ⟨110⟩ direction. The corner-connected octahedral array represents the $(Mg_{0.24}Nb_{0.76})_2O_6$ sub-structure. The toroids of flat ellipsoids represent the six equivalent 96h A-site positions of the O′$(Bi_{0.833}Mg_{0.11})_2$ sub-structure. The tetrahedral clusters of ellipsoids represent the four equivalent 32e site positions for the displaced O′ oxygens. (b) Shows an expanded view of one particular O′$(Bi_{0.833}Mg_{0.11})_4$ tetrahedron.

A-site ions again takes a flat pancake shape so that the six 96h A-site ions virtually overlap to form a squashed donut shape perpendicular to the local O′–A–O′-axis (see Fig. 2).

At this last stage of the refinement, the assumptions that there were no oxygen vacancies and that the metal ion vacancies would be located exclusively on the A-site positions were tested by allowing the oxygen occupancies to vary without constraints and by refining the relative occupancies of the Mg/Ni ions on the A and B sites. The relative oxygen occupancies were refined first. The occupancy on the O(1) refined to 1.000(4) while that on the O′ site refined to 0.97(2) for BMN and to 1.000(3) and 0.99(2) for BNN, i.e. to within error there is no evidence for oxygen vacancies on either the O or O′ sites. The relative M occupancies on the A and B sites were refined next but again changed very little (and in the unphysical direction of having more than one metal ion on the pyrochlore B site) as did the refinement statistics, e.g. for BMN, the Mg occupancy on the A site refined to 0.10 (down from the initial 0.11) while the Mg occupancy on the B site refined to 0.25 (up from the initial 0.24). Clearly the vacancies on the metal atom sites are overwhelmingly if not entirely located on the A sites. There was thus no evidence for any need to

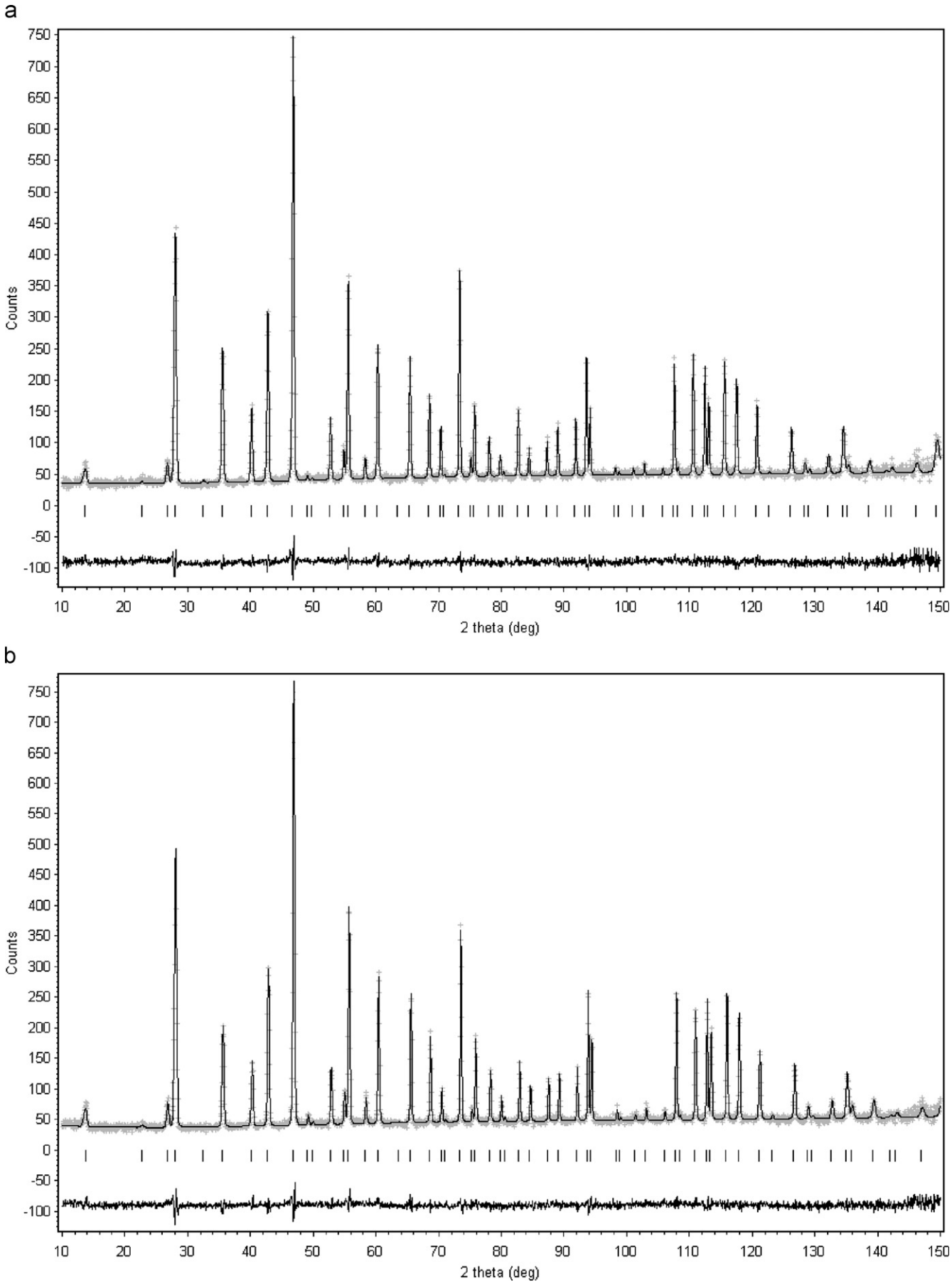

Fig. 3. The final resultant neutron powder profile fits for (a) BMN and (b) BNN. Both plots show the data, fits as well as the difference profiles for the refinements.

change the assumptions underlying Model 4 which was therefore taken as the final refinement model.

The final refinement results using model 4 are given in Tables 1 and 2. The final difference profiles are shown in Fig. 3 while the final displacively disordered average structure for BMN is shown in Fig. 2. There are clearly strong qualitative similarities with the recently reported average structures of other Bi-pyrochlores [7–9,11–13] cf., for example, Fig. 2 with Figs. 4 and 5 of [12]. Nonetheless, subtle differences, in particular the relative magnitudes of the refined displacement magnitudes off the 16*d* and 8*b* sites for the *A* and O′ sites of the various Bi-pyrochlores remain.

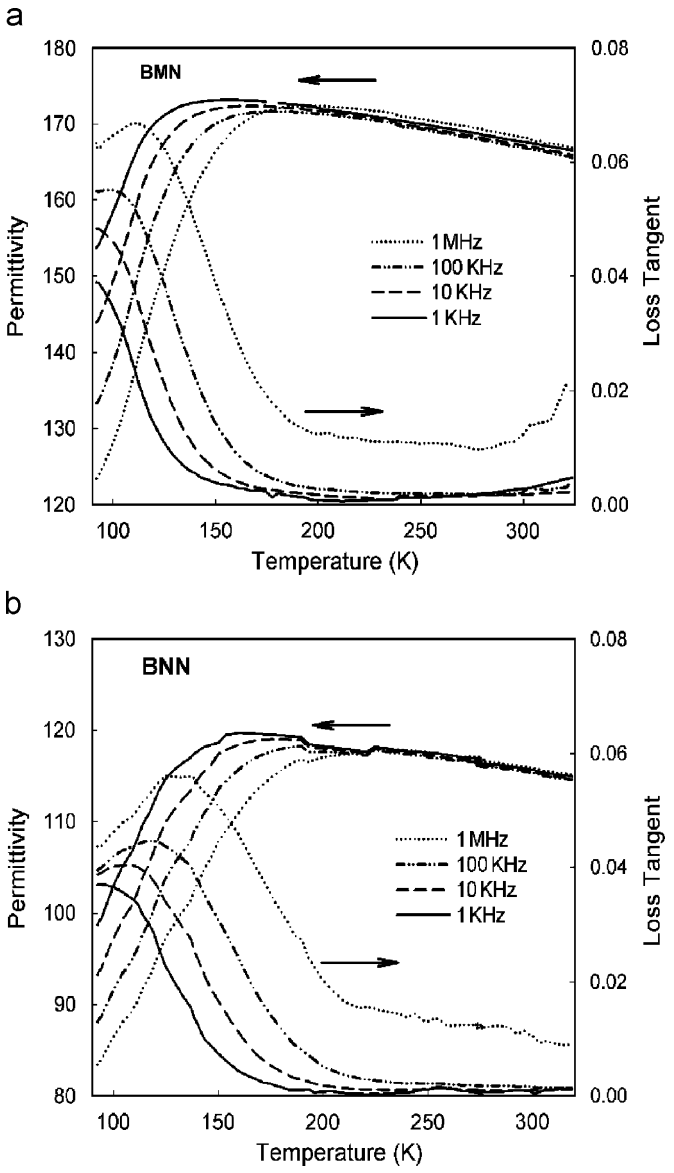

Fig. 4. The measured dielectric permittivities as well as dielectric loss tangents of the BMN and BNN samples as a function of applied frequency at 1, 10, 100 kHz and 1 MHz as a function of temperature from ~325 K down to liquid nitrogen temperature, i.e. ~90 K ((a) for BMN, (b) for BNN).

3.2. Dielectric properties

The measured dielectric permittivities and dielectric loss tangents of the BMN and BNN samples at 1, 10, 100 kHz and 1 MHz as a function of temperature from ~325 K down to liquid nitrogen temperature, i.e. ~90 K is shown in Fig. 4. The low temperature frequency dispersive behaviour characteristic typical of Bi-pyrochlores is clearly apparent [2,12,16,17] with the maximum in both the dielectric permittivity and the dielectric loss tangent moving to higher temperature with increased measurement frequency. Note that the peak in the dielectric loss curve at 1 MHz occurs at T_m~112 K in the case of BMN and at ~130 K in the case of BNN. At 1 MHz, the maximum in the dielectric permittivity is ~172 at ~190 K in the case of BMN and ~118 at ~220 K in the case of BNN. In the case of BNN, there is some indication that that the dielectric loss versus temperature curve below T_m does not simply reduce towards zero on further lowering of temperature but rather may be entering a plateau region in the vicinity of the lowest temperature obtainable. Lower temperature dielectric measurements, however, are needed to confirm whether or not this is indeed the case.

4. Conclusions

While the refined disordered *average* structures given in Tables 1 and 2 for $Bi_{1.667}Mg_{0.70}Nb_{1.52}O_7$ (BMN) and $Bi_{1.667}Ni_{0.75}Nb_{1.5}O_7$ (BNN) are by no means sufficient to define the different local configurations and associated displacive relaxations possible, they are nonetheless important as they define the broad structural parameters within which any modelling of the local structure must necessarily operate, e.g. the displacive shifts of the local *A*-site cations away from the ideal pyrochlore *A*-site positions should be of magnitude ~0.41 Å for both BMN and BMN and directed perpendicular to the local O′–*A*–O′-axis. Likewise, any proposed local ordering of the Bi^{3+}, Mg^{2+}/Ni^{2+} and □'s on the *A* sites as well as of the Mg^{2+}/Ni^{2+} and Nb^{5+} on the neighbouring *B*-site positions must explain why the *A* ion shifts induced by the local chemistry are necessarily perpendicular to the local O′–*A*–O′-axis.

In the case of BZN and BZN-related Bi-pyrochlores, where the concentration of the small, heavily under-bonded M^{II} = Zn ions on the pyrochlore *A* site approaches 25% and where the concentration of □'s on the *A* sites is sufficiently small, we have recently suggested a crystal chemically reasonable explanation in terms of $\frac{1}{4}\langle 112\rangle$ inter-tetrahedral Zn–Zn separation distances from one O′Bi_3Zn tetrahedra to the next (see e.g. Fig. 6 of [14]). In the cases of BMN and BNN, however, where the concentration of the small, heavily under-bonded *M* = Mg or Ni ions on the pyrochlore *A* site is much more like 11–12% rather than 25% and where the concentration of □'s on the *A* sites is ~5%, the explanation for the observed highly anisotropic displacive disorder on the *A* site is not so

obvious. The structured diffuse scattering recently shown to be characteristic of BMN and BNN [20] shows that β-crystobalite-like $O'A_2$ tetrahedral edge rotation modes play an important role.

The severe underbonding (~60%) of the small Mg/Ni ions on the pyrochlore A site of BMN or BNN [20], regardless of whether or not they are presumed to displace perpendicular to the local O′–A–O′-axis or not [15,20], can clearly only be remedied by O′ displacements directed towards the Mg/Ni ions. Crystal chemical considerations suggest that the magnitude of these shifts need to be substantial, ~0.5 Å in the case of BMN and BNN [20]. The refined O′ shift from Tables 1 and 2 are a bit smaller at ~0.35 Å/~0.37 Å. Note, however, that these latter shifts represent the centres of rather large displacement ellipsoids (see e.g. Fig. 2b). The presence of ~5% □'s on the A sites, however, complicates matters considerably. When an O′ ion is surrounded by either 4 Bi's of 3 Bi's and one Mg or Ni ion (the most likely local configurations), the centreing O′ ion is either happily bonded or over-bonded implying that the significantly under-bonded Bi and heavily under-bonded Mg or Ni ions cannot improve their under-bonding by moving closer to the O′ ions but must instead move perpendicular to the local O′–A–O′-axis [20]. When an O′ ion is surrounded by 3 Bi's and one □ (a reasonably common likelihood), however, the centreing O′ ion will be under-bonded (see Tables 5 and 6 of [20]) and hence will move away from the □ and towards the remaining three Bi ions.

It is no trivial matter to put all the above considerations together into a coherent picture of these "… misplaced-displacive cubic pyrochlore …" phases. It seems clear, however, that both the concentration of M-site ions as well as □'s on the pyrochlore A sites play critical roles and that the dielectric relaxation properties of such Bi-pyrochlores are intimately dependant upon this local crystal chemistry.

Acknowledgments

B.N., Y.L. and R.L.W. acknowledge financial support from the Australian Research Council (ARC) in the form of an ARC Discovery Grant. The Authors would also like to thank the Australian Institute of Nuclear Science and Engineering for their financial support (AINSE Award 2006, Grant AINGRA06250).

References

[1] D. Liu, Y. Liu, S.Q. Huang, X. Yao, J. Am. Ceram. Soc. 76 (1993) 2129–2132.
[2] D.P. Cann, C.A. Randall, T.R. Shrout, Solid State Commun. 100 (1996) 529–534.
[3] X. Wang, H. Wang, X. Yao, J. Am. Ceram. Soc. 80 (1997) 2745–2748.
[4] M. Valant, P.K. Davies, J. Am. Ceram. Soc. 83 (2000) 147–153.
[5] W. Ren, S. Trolier-McKinstry, C.A. Randall, T.R. Shrout, J. Appl. Phys. 89 (2001) 767–774.
[6] J. Lu, S. Stemmer, Appl. Phys. Lett. 83 (2003) 2411–2413.
[7] I. Levin, T.G. Amos, J.C. Nino, T.A. Vanderah, C.A. Randall, M.T. Lanagan, J. Solid State Chem. 168 (2002) 69–75.
[8] R.L. Withers, T.R. Welberry, A.K. Larsson, Y. Liu, L. Norén, H. Rundlöf, F.J. Brink, J. Solid State Chem. 177 (2004) 231–244.
[9] B. Melot, E. Rodriguez, Th. Proffen, M.A. Hayward, R. Seshadri, Mater. Res. Bull. 41 (2006) 961–966.
[10] T.A. Vanderah, I.L. Levin, M.W. Lufaso, Eur. J. Inorg. Chem. 14 (2005) 2895–2901.
[11] T.A. Vanderah, M.W. Lufaso, A.U. Adler, I. Levin, J.C. Nino, V. Provenzano, P.K. Schenk, J. Solid State Chem. 179 (2006) 3467–3477.
[12] M.W. Lufaso, T.A. Vanderah, I.M. Pazos, I. Levin, R.S. Roth, J.C. Nino, V. Provenzano, P.K. Schenk, J. Solid State Chem. 179 (2006) 3900–3910.
[13] T.A. Vanderah, T. Siegrist, M.W. Lufaso, M.C. Yeager, R.S. Roth, J.C. Nino, S. Yates, Eur. J. Inorg. Chem. 23 (2006) 4908–4914.
[14] Y. Liu, R.L. Withers, T.R. Welberry, H. Wang, H. Du, J. Solid State Chem. 179 (2006) 2141–2149.
[15] V. Krayzman, I. Levin, J.C. Woicik, Chem. Mater. 19 (2007) 932–936.
[16] J.C. Nino, M.T. Lanagan, C.A. Randall, J. Appl. Phys. 89 (2001) 4512–4516.
[17] S. Kamba, V. Porokhonskyy, A. Pashkin, V. Bovtun, J. Petzelt, J.C. Nino, S. Trolier-McKinstry, M.T. Lanagan, C.A. Randall, Phys. Rev. B 66 (2002) 054106.
[18] M. Valant, D. Suvorov, J. Am. Ceram. Soc. 88 (9) (2005) 2540–2543.
[19] V.P. Sirotinkin, A.A. Bush, Inorg. Mater. 39 (2003) 974–977.
[20] B. Nguyen, Y. Liu, R.L. Withers, J. Solid State Chem. 180 (2007) 554–562.
[21] Sietronics Pty Ltd., P.O. Box 3066, Belconnen, ACT 2617, Australia.
[22] B. Noläng, Inst. Materialkemi, Ångströmlaboratoriet, Box 538, S-751 21 Uppsala, Sweden.
[23] 〈http://www.ansto.gov.au/ansto/bragg/hifar/hrpd.html〉.
[24] B.A. Hunter, Rietica—A Visual Rietveld Program, Commission on Powder Diffraction Newsletter, vol. 20, 1998, p. 21.